2009

Optimal Thresholds of Feature Tracking for Blood Velocity and Tissue Motion Estimation

Tiantian Xu
University of Nebraska-Lincoln

Gregory R. Bashford
University of Nebraska-Lincoln, gbashford2@unl.edu

Optimal Thresholds of Feature Tracking for Blood Velocity and Tissue Motion Estimation

Tiantian Xu and Gregory R. Bashford

***Abstract*—Feature tracking is an algorithm for estimating blood flow velocity and tissue motion using pulse-echo ultrasound. In contrast to cross-correlation speckle-tracking techniques, feature tracking identifies features at discrete locations and corresponds them from frame to frame. Prior studies have demonstrated that feature-tracking estimates exhibit lower variance than those obtained by the conventional autocorrelation method and require less computational complexity than either speckle tracking or autocorrelation. To date, not much attention has been paid to the process by which trackable features (normally local maxima) are selected from the set of all available features. In the selection process, it is desired to minimize flow estimate variance while providing sufficient spatial and temporal coverage of flow area. Flow studies were performed with a blood flow phantom, 3.5-MHz spherically focused transducer, and a pulser/receiver. Values were selected for the amplitude threshold (based on the RMS value) and width thresholds (based on the wavelength corresponding to transducer center frequency). The performance of this method using different threshold values was evaluated by the estimate standard deviation and number of features available to track. Results show that an optimal width threshold occurs at about 40 to 45% of the transmission wavelength, while a trade-off exists between amplitude thresholds and spatial flow field coverage. Both the standard deviation of estimated velocities and number of available features decrease with increasing threshold (either amplitude or width). This affords a user a method of determining optimal feature tracking thresholds depending on the specific flow application. Judicious selection of feature thresholds can decrease the estimate standard deviation by more than 25%.**

I. Introduction

Ultrasound has been widely used as a diagnostic tool in the cardiovascular system. It is known that the distribution of the blood velocities within a vessel contains valuable diagnostic information. Likewise, motion of heart tissue is dependent on the health of cardiac muscle [1]. Thus, accurate measurement of blood flow velocity and tissue motion is useful to clinicians.

Several methods have been used to develop ultrasound motion estimators. Conventional methods (available on most commercial ultrasound machines) operate in 1-D and estimate the velocity vector projection along the axial dimension of the ultrasound beam. These fall into 2 main classes. The first class includes those that derive from the autocorrelation estimator [2], meant to estimate the mean flow velocity quickly over a larger spatial field of view, and now commonly referred to as color flow. The second class includes those that display a spectral plot of the (temporal- and wall-filtered) flow signal [3], meant for visualizing a velocity distribution at a single (resolution-limited) small region of interest, now commonly referred to as "spectral Doppler."

Many researchers have formed alternate estimation algorithms. Here, only a few are mentioned; more complete literature reviews are available elsewhere [4], [5]. Multiple transducers can provide flow information in more than one dimension if the transducers are mounted favorably; in this approach, the velocity vector is obtained at one location in space but not over a broad field of view [6]–[8]. Multiple subapertures within a single transducer may substitute for additional transducers [9]. Estimating the transit time across the ultrasound beam was proposed for measuring flow parallel to the transducer face [10]. The spatial quadrature technique was proposed to estimate lateral motion by employing a modulation in the acoustical field in the lateral direction [11], [12]. Time-domain cross-correlation of successive pulsed interrogations has been validated and a real-time system developed in 2 dimensions [13]–[15]. Maximum-likelihood estimators have also been proposed [16], [17].

Feature tracking was first proposed by Roundhill in 1991 and performed accurately in one dimension [18]. Instead of dealing with the entire volume of image data, feature tracking selects discrete trackable locations in the data, which are called features. Directly tracking selected features permits estimation of the direction and velocity of target motion. This method significantly reduces data storage and increases computational efficiency [19]. Feature tracking was extended to ultrasound 3-D velocity and motion measurement [19], [20].

Most recently, to assess the performance of feature tracking in terms of estimation bias and standard deviation, it was directly compared with the conventional autocorrelation method. The results suggested that feature tracking exhibits a comparable estimation mean to the conventional commercial method and a favorable estimation variance [21].

Feature extraction is the first and crucial step in feature tracking. First, a candidate list of features is created based on applying a rule to the data (e.g., finding the locations of local maxima of the signal amplitude). Next, the candidate list is narrowed according to some criterion (e.g., the features must meet a certain threshold amplitude). Prior studies used an ad hoc approach to set thresholds based on experimental observation [19]–[22]. Specifically, in [20], an amplitude threshold was used to select features

Manuscript received October 31, 2008; accepted July 22, 2009.

The authors are with the Department of Biological Systems Engineering, University of Nebraska-Lincoln, Lincoln, NE (e-mail: gbashford2@unl.edu).

Digital Object Identifier 10.1109/TUFFC.2009.1353

with amplitude above the average magnitude of the pulse-echo signal. Additionally, a width threshold was established to extract features with a certain breadth in the time domain. The width threshold was 1/4 to 1/3 of the wavelength corresponding to the center frequency of the transducer. In [22], Morsy and von Ramm proposed different methods to select thresholds; the amplitude threshold H_{th} was determined by the equation

$$H_{\text{th}} = \mu_A + C \cdot \sigma_A, \tag{1}$$

where μ_A is the mean of the detected axial line, and σ_A is its standard deviation. C is a number used to control the value of H_{th}. Also, 2 width thresholds W_{min} and W_{max} were selected. W_{min} represents a lower limit on the acceptable width of the axial segment while W_{max} represents an upper threshold on the axial segment width. The values used for W_{min} and W_{max} were 2 samples (0.3 mm) and 11 samples (1.7 mm). Based on these 2 thresholds, the candidate list of features was narrowed. Morsy and von Ramm found that by raising the thresholds, the number of available features declined. This work represented a step toward standardization of threshold selection, but was not fully developed.

Thus, to date, not much attention has been paid to either the process by which trackable features are selected from the data or the process by which the candidate list is narrowed. Although both processes are clearly important, here we address the latter, i.e., we suggest the use of amplitude and width thresholds and study the relationship between threshold selection and estimate performance. The reason that we are studying the latter process in this paper is that we have previously shown that at least one feature (the local maxima) translates in correspondence with tissue motion [20]; rather than studying multiple processes at once, we wish to explore how thresholds affect the accuracy of the motion estimation. The process by which trackable features are selected from data will be the focus of future research.

The number of trackable features will decrease as the amplitude or width threshold increases. We hypothesize that with a higher threshold, the estimate standard deviation (error) will decrease. However, tracking fewer features would result in sparser spatial sampling of the flow field. Therefore, there should be a trade-off between spatial sampling of motion (number of trackable features) and the accuracy of estimation at each spatial location. If this hypothesis is true, it should be possible to find optimal thresholds that maximize the estimator's accuracy (minimize the standard deviation) for a desired spatial sampling.

The purpose of this paper is to compare feature-tracking estimation standard deviation with varying width and amplitude thresholds. This analysis will be done in one dimension. Future studies will address motion estimation in multiple dimensions, where it is expected new challenges will arise in feature selection and tracking and thus will require further study.

II. Materials and Methods

The experimental setup was similar to the one used in our previous studies [21] and is briefly described here. A commercial flow phantom (Optimizer RMI 1425, Gammex, Middleton, WI) was used to simulate blood flow. This phantom contains a tube (5 mm inside diameter, 1.25 mm thickness) through which blood-mimicking fluid is pumped. The fluid has acoustic properties similar to blood (speed of sound 1550 m/s, density 1.03 g/mL). The tube is surrounded by tissue-mimicking material (speed of sound 1540 m/s, attenuation 0.5 dB/cm/MHz). A spherically focused 3.5-MHz transducer with F# = 3.0 and −6 dB bandwidth = 35% (A382S, Panametrics, Waltham, MA) was mounted on a transducer stand and vertically directed at the blood flow phantom. The tube is oriented at a 40-degree angle to the horizontal, i.e., to the transducer face. Due to physical limitations combining the focal length of the transducer and the location of the tube interrogated past the pump, the flow was not guaranteed to be fully developed (parabolic) by the manufacturer; however, experiments (see Results section) showed that the detected flow was nearly parabolic. The study of how threshold selection affects other types of flow (such as plug or turbulent) is outside the scope of this paper.

The SNR in the experimental setup was 15.0 dB. The SNR was measured in the following manner. One thousand pulse-echo signals were acquired with the flow phantom velocity set to zero. The average of the 1000 signals was calculated to estimate the mean signal. Then, for each signal, a noise signal was produced by subtracting the mean signal from the raw signal. The SNR was calculated by dividing the standard deviation of the mean signal by the standard deviation of the noise signal.

A pulser/receiver (500PR, Panametrics) was used to excite the transducer. The phantom was set to constant velocity mode with velocities of 15, 30, 45, and 60 cm/s. The PRF was set at 4 times the effective Doppler frequency, given the phantom velocity and scan geometry. Our motivation for picking this PRF was to place the center of the resulting Doppler spectrum halfway between 0 Hz and PRF/2 Hz to avoid aliasing. The resulting PRFs were 2090, 4170, 6330, and 6720 Hz, respectively. (The pulser in our lab has a maximum PRF of 6720 Hz, so the 60 cm/s data were taken at 3.2 times the effective Doppler frequency. This did not appreciably change the results.) Each data set consisted of 128 pulse-echo interrogations separated by a time interval of 1/PRF. Each pulse-echo signal consisted of 20.5 μs of data centered about and fully including the phantom tube. The echo signal was received by a dedicated 14-bit, 100-MHz A/D card (PXI-5122, National Instruments, Austin, TX). In feature-tracking processing, only data corresponding to the tube (6.5 μs) were analyzed.

Filtering in the time direction was performed with a 12th-order Butterworth IIR band pass filter (−3-dB cutoff frequencies 1.89 and 5.29 MHz). No initialization was used in the band pass filter and no samples were discarded

because the samples corresponding to the tube were at least several hundred samples from the start of the signal. In the ensemble ("slow time") direction, a 2nd-order Butterworth IIR high pass filter (wall filter) was designed (−3-dB cutoff frequency = 6.3% of PRF/2) to cancel stationary echoes and applied to the data. No initialization was used in the wall filter because the first 10 samples were discarded.

Estimates of the probability distribution functions for feature amplitude and width were made by forming histograms of detected local maxima over several data sets. Specifically, 20 data sets each containing 128 pulse-echo A-lines were examined for each estimate. A feature was detected by examining successive samples x_i along each line and looking for local maxima (peaks). If x_i satisfies

$$x_{i-1} < x_i \quad \text{and} \quad x_i > x_{i+1}, \tag{2}$$

then the location x_i was considered a feature. The amplitude and full-width at half-maximum (FWHM) of the peak were then recorded to calculate the cumulative probability for each value.

Two sets of thresholds were chosen. The first set (set 1) spanned the cumulative distribution of available features from 10 to 90% in multiples of 10% for both amplitude and width thresholds. In the second set (set 2), amplitude thresholds were chosen in even fractions of the mean energy (RMS) of the signal, while width thresholds were chosen in even fractions of the wavelength of the center frequency of the transducer.

A portion of the RF signal corresponding to the tube location was culled for all features. Each feature was examined to see if it met an amplitude and time (width) threshold. Those features that remained were tracked across 8 pulse-echo repetitions (selected contiguously from the 128 A-lines, i.e., 8 adjoined lines separated in time by the PRF). To ensure that features were tracked across the entire tube, the diameter of the tube was divided into 8 equal distances. At least 100 features were tracked at each of these 8 locations (depths) within the tube. The performance of feature tracking under these conditions was evaluated by calculating the mean velocity and standard deviation of the estimates.

III. Results

Histograms of the cumulative probability of the amplitude and width of the features are shown in Fig. 1 for all velocities. Markers on each curve show the actual threshold values selected in our experiment for set 2. The set 1 values can be determined by noting where the cumulative probability curves cross the horizontal grid lines.

Graphs of the estimate standard deviation versus width thresholds are shown in Fig. 2. Fig. 3 denotes the standard deviation versus different amplitude threshold values. Graphs of the number of trackable features found in one data set versus threshold values are shown in Fig. 4.

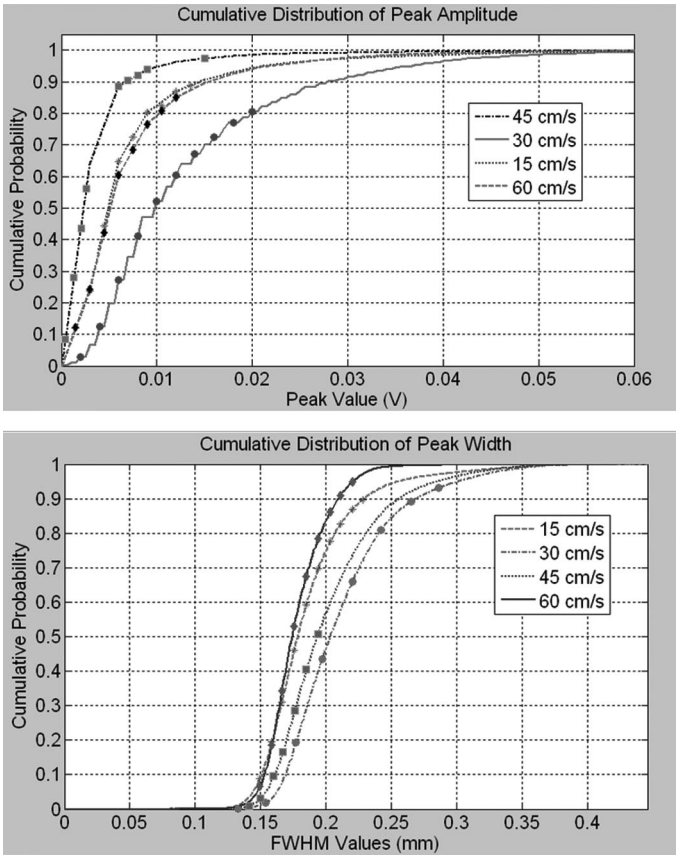

Fig. 1. Cumulative distribution of features: (top) feature amplitude, (bottom) feature width. Markers are shown where chosen threshold values for set 2 were used in the experiments.

The mean estimated velocity throughout the tube is shown in Fig. 5 for all 4 velocity experiments. It was not possible to assume a particular flow profile *a priori*, so to compare the volume flow rate displayed on the phantom's controller with that which would be estimated by feature tracking, we adopted a quasinumerical technique by integrating the mean velocity detected in the tube across a cross-sectional circle. That is, the cross-sectional area in the tube was divided into 8 concentric sectors, each with a width of 1/8 of the tube's inner diameter. Each of the 8 velocities v_i detected across the tube was assumed to correspond to one of the sectors S_i, thus representing a fraction of the entire volume flow. The flow rate was calculated as follows:

$$F = \sum_{i=1}^{8} (v_i \times S_i). \tag{3}$$

Using the mean velocity distribution denoted by Fig. 5, we calculated the flow rate for the velocity settings of 15, 30, 45, and 60 cm/s to be 1.1, 2.9, 4.2, and 5.5 mL/s, respectively. These results are close (within about 10%) to the values given by the phantom, which are 1.0, 2.6, 4.2, and 5.9 mL/s, respectively. The motivation for comparing the volume flow rates were to check the estimated mean velocities, which cannot be compared directly with the

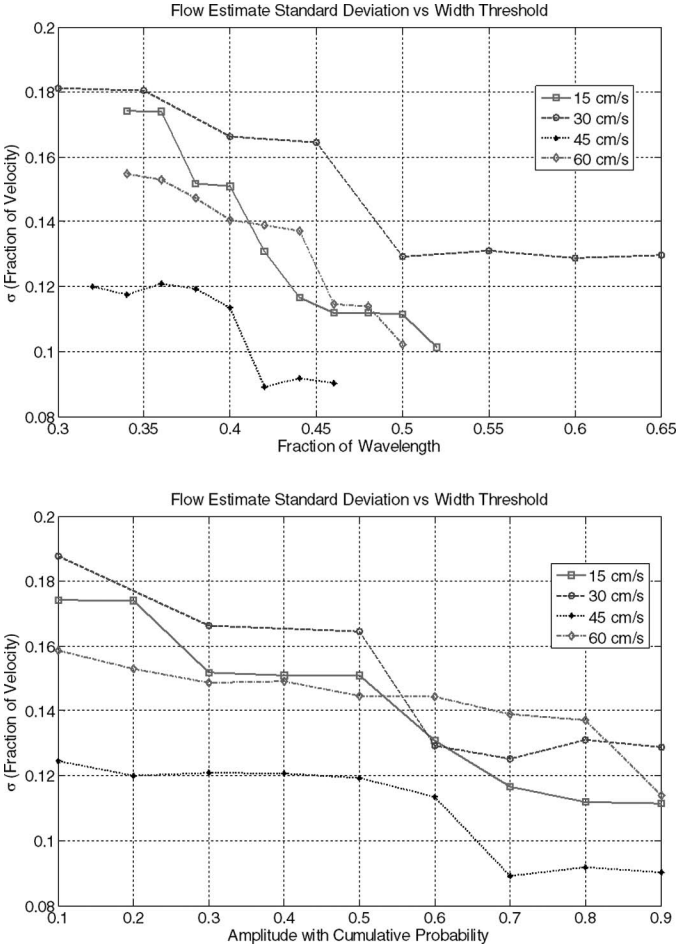

Fig. 2. Standard deviation versus width thresholds: (top) thresholds with constant interval of wavelength fractions (set 2 thresholds); (bottom) thresholds with constant interval of cumulative probability (set 1 thresholds).

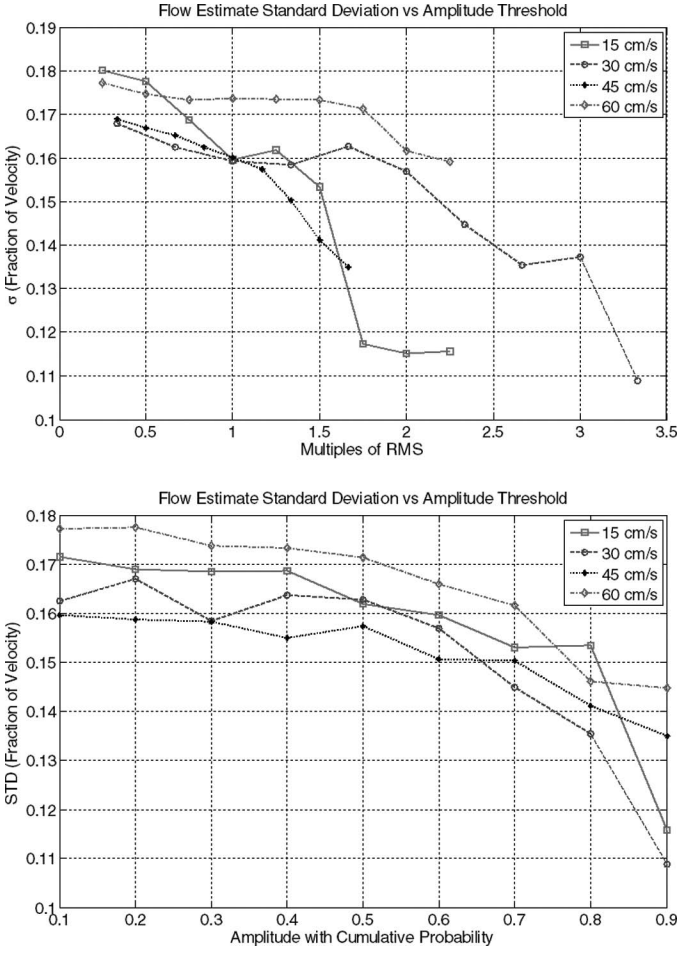

Fig. 3. Standard deviation versus amplitude thresholds: (top) thresholds with constant intervals of RMS widths (set 2 thresholds); (bottom) thresholds with constant interval of cumulative probability (set 1 thresholds).

flow phantom setting because only one velocity for the tube is selectable.

Another important note is that flow estimation is seen slightly outside the boundaries of the inner diameter of the tube in Fig. 5 because of convolution effects with the pulse length (detected full-width-at-half-maximum measured to be 1.3 microseconds or 1.0 mm).

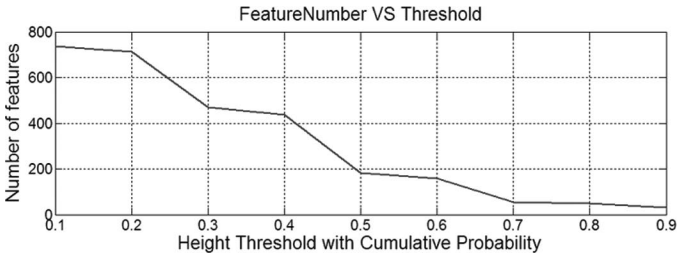

Fig. 4. Number of trackable features versus amplitude threshold values.

IV. Discussion

The relationship between estimation standard deviation and threshold value reveals that, as expected, the standard deviation decreases with higher threshold values. An interesting finding is that in the width threshold curves, a significant drop occurs at a certain point for most velocities. For example, in the top of Fig. 2, the 30-cm/s curve standard deviation remains between 0.16 and 0.18 of the velocity (between 4.8 and 5.4 cm/s) up to a fraction of a wavelength of about 0.45. At that point, the curve suddenly drops to about 0.13 of the velocity (3.9 cm/s), which is an improvement of more than 25%. The same or close behavior can be seen in the other velocities as well. For all 4 velocities, this transition point occurs at a threshold between 0.40 and 0.45 of a wavelength. This drop suggests that a nonlinear relationship exists between estimate standard deviation and threshold selection. The reason for this sudden drop may be related to the distribution of the sizes of features within the speckle data set and is indicated for future study. However, a user can presently take advantage of this transition point to minimize estimate variance while preserving flow field coverage over time as explained below.

The relationship between amplitude threshold and standard deviation denoted by Fig. 3 is different, with

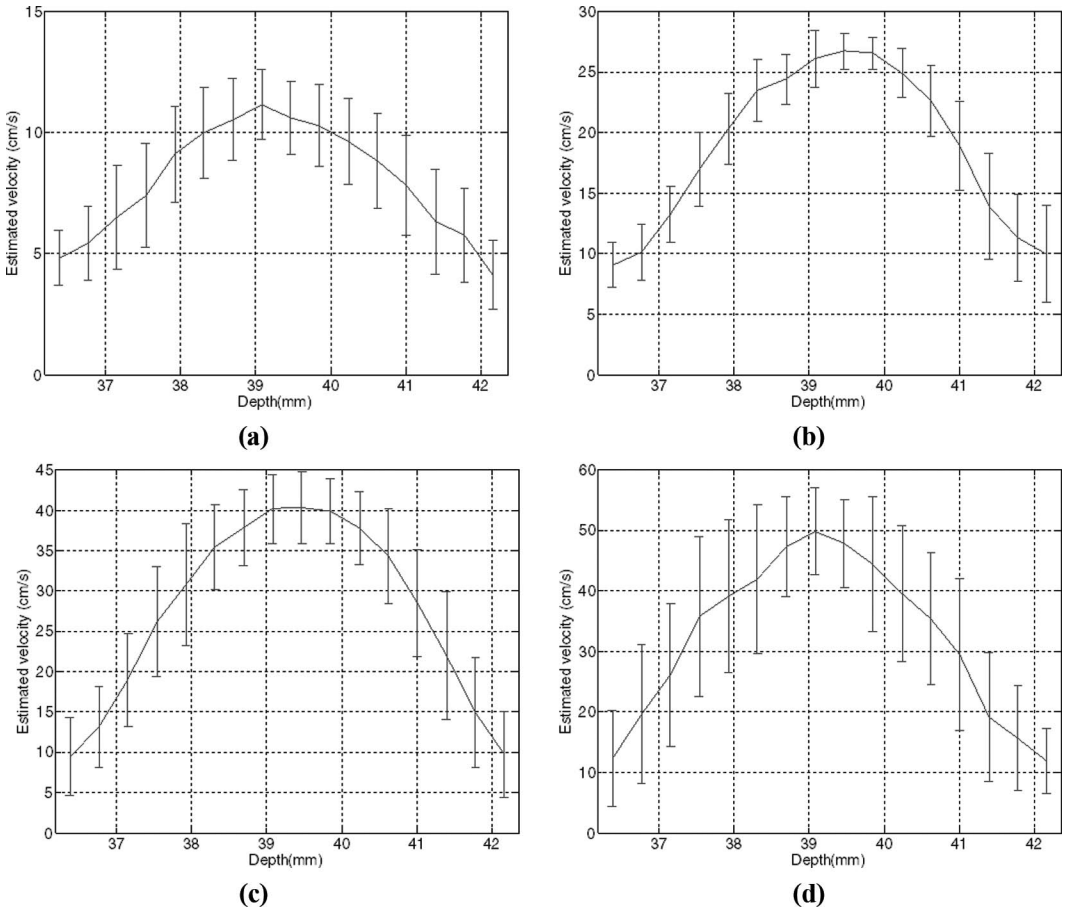

Fig. 5. Estimated velocity across the tube: (a)15 cm/s, (b) 30 cm/s, (c) 45 cm/s, and (d) 60 cm/s.

no consistent behavior or transition point when thresholds are viewed as multiples of RMS. However, from Fig. 3 (bottom), the standard deviation curves are markedly similar when comparing thresholds chosen across the cumulative distribution.

From the relation of standard deviation and threshold, we can generally say that greater thresholds give a better estimation through a lower standard deviation. The range of potential improvement can be significant. For example, the maximum and minimum standard deviations in the 30-cm/s curve on Fig. 3 are 5.04 and 3.26 cm/s, an improvement of more than 35%.

The number of trackable features decreases with an increase of threshold values, which is shown in Fig. 4. This is important because it shows how finely the flow estimate space in the tube will be sampled. For 1-D estimation, we are sampling across a line running transverse to the tube in the ultrasound beam direction. Higher thresholds result in fewer trackable features, meaning sparser coverage of the flow estimate space. The benefit of a higher threshold is a smaller estimate standard deviation, which translates to higher accuracy. On the other hand, a smaller threshold gives a greater number of trackable features, meaning more coverage of the flow space, but greater estimate standard deviation, which translates to less accuracy. The required sampling relates to the expected spatial flow field correlation [16]. The actual flow field coverage as a function of space and time for different threshold selection is a topic outside the scope of this paper, but is indicated for future study.

These graphs may help the interested user select optimal thresholds for a particular application. For example, the data shown in Fig. 2 suggest that rapid improvement (decrease) in standard deviation occurs while increasing the threshold until a particular transition point, where not much further improvement can be expected. In particular, using width thresholds at about 40 to 45% of the center frequency wavelength gives optimal results by taking advantage of the rapid decrease in standard deviation while avoiding the region where estimation variance stays relatively constant. Fig. 3 suggests that using the largest practical amplitude threshold provides the lowest estimate variance. These selections must be balanced with the desired sampling of the flow space and desired time to acquire estimates. Although (as noted above) a comprehensive study of space/time coverage of features in the flow field as functions of threshold selection and flow profile has not been done, the current results can help those applications with some *a priori* known flow profiles. If the flow application is in an area that is not expected to vary widely throughout the flow space, such as plug flow, then higher thresholds with less flow field sampling and higher accuracy are preferable. On the other hand, if the flow application is expected to have a greater variance across

space, such as turbulent flow, lower thresholds would be better for sufficient coverage of the flow field. It should be noted that another factor in this process is time to acquire samples. If more time is available to collect feature-tracking data, then one can afford to wait for a sufficient number of thresholded features to appear. Therefore, taking into account the factors of desired spatial flow field coverage, desired flow estimation accuracy (variance), and desired time to complete flow sampling, a user can optimize the feature-tracking algorithm for a particular application.

V. Conclusion

This paper investigated the relationship between feature-tracking estimation performance and feature threshold values. The number of trackable features decreases with increasing thresholds. The decrease of standard deviation with width thresholds suggests that an optimal width threshold occurs at about 40 to 45% of the center frequency wavelength. The decrease of standard deviation with amplitude thresholds does not contain a similar type of transition point. Combining the relationship between the number of trackable features and estimate standard deviation, users may select preferred threshold values according to the specific flow application. With a judicious choice of thresholds, the estimated standard deviation can be increased 20 to 35%. Further study should include the extension of this analysis to multiple dimensions, as well as a cross-analysis (simultaneous varying of amplitude and width thresholds) to evaluate flow estimation performance. Also, the relationship between flow field coverage (feature existence) in space and time for different flow profiles should be examined.

References

[1] I. A. Hein and W. D. O'Brien Jr. "Current time-domain methods for assessing tissue motion by analysis from reflected ultrasound echoes—A review," *IEEE Trans. Ultrason. Ferroelectr. Freq. Control*, vol. 40, no. 2, pp. 84–102, Mar. 1993.

[2] C. Kasai, K. Namekawa, A. Koyano, and R. Omoto, "Real-time two-dimensional blood flow imaging using an autocorrelation technique," *IEEE Trans. Sonics Ultrason.*, vol. 32, no. 3, pp. 458–463, 1985.

[3] D. H. Evans, W. N. McDicken, R. Skidmore, and J. P. Woodcock, *Doppler Ultrasound: Physics, Instrumentation, and Clinical Applications.* New York: John Wiley & Sons, 1989.

[4] J. A. Jensen, *Estimation of Blood Velocities Using Ultrasound: A Signal Processing Approach.* Cambridge: Cambridge University Press, 1996.

[5] P. R. Hoskins, "A review of the measurement of blood velocity and related quantities using Doppler ultrasound," *Proc.- Inst. Mech. Eng.*, vol. 213, no. 5, pp. 391–400, 1999.

[6] M. D. Fox, "Multiple crossed-beam ultrasound Doppler velocimetry," *IEEE Trans. Sonics Ultrason.*, vol. SU-25, no. 5, pp. 281–286, 1978.

[7] I. A. Hein, "3-D flow velocity vector estimation with a triple-beam lens transducer—Experimental results," *IEEE Trans. Ultrason. Ferroelectr. Freq. Control*, vol. 44, no. 1, pp. 85–95, Jan. 1997.

[8] D. Vilkomerson, T. Chilipka, A. Nazarov, M. Kuhlmann, and N. W. Levin, "Non-specialist ultrasound measuring of access flow: New technology," *Blood Purif.*, vol. 22, no. 1, pp. 78–83, 2004.

[9] P. J. Phillips, A. P. Kadi, and O. T. von Ramm, "Feasibility study for a two-dimensional diagnostic ultrasound velocity mapping system," *Ultrasound Med. Biol.*, vol. 21, no. 2, pp. 217–229, 1995.

[10] V. L. Newhouse, D. Censor, T. Vontz, J. A. Cisneros, and B. B. Goldberg, "Ultrasound Doppler probing of flows transverse with respect to beam axis," *IEEE Trans. Biomed. Eng.*, vol. BME-34, no. 10, pp. 779–789, 1987.

[11] M. E. Anderson, "Multi-dimensional velocity estimation with ultrasound using spatial quadrature," *IEEE Trans. Ultrason. Ferroelectr. Freq. Control*, vol. 45, no. 3, pp. 852–861, May 1998.

[12] J. A. Jensen and P. Munk, "A new method for estimation of velocity vectors," *IEEE Trans. Ultrason. Ferroelectr. Freq. Control*, vol. 45, no. 3, pp. 837–851, May 1998.

[13] G. E. Trahey, J. W. Allison, and O. T. von Ramm, "Angle independent ultrasonic detection of blood flow," *IEEE Trans. Biomed. Eng.*, vol. BME-34, no. 12, pp. 964–967, 1987.

[14] L. N. Bohs, B. H. Friemel, B. A. McDermott, and G. E. Trahey, "Real-time system for angle-independent US of blood flow in two dimensions: Initial results," *Radiology*, vol. 186, no. 1, pp. 259–261, Jan. 1993.

[15] P. M. Embree and W. D. O'Brien, Jr., "The accurate ultrasonic measurement of the volume flow of blood by time domain correlation," in *Proc. IEEE Ultrasonics Symp.,* 1985, pp. 963–966.

[16] M. Schlaikjer and J. A. Jensen, "Maximum likelihood blood velocity estimator incorporating properties of flow physics," *IEEE Trans. Ultrason. Ferroelectr. Freq. Control*, vol. 51, no. 1, pp. 80–92, Jan. 2004.

[17] K. W. Ferrara and V. R. Algazi, "A new wideband spread target maximum likelihood estimator for blood velocity estimation—Part I: Theory," *IEEE Trans. Ultrason. Ferroelectr. Freq. Control*, vol. 38, no. 1, pp. 1–15, Jan. 1991.

[18] D. N. Roundhill, "Ultrasound time domain velocity measurement," Ph.D. dissertation, Duke Univ., Durham, NC, 1991.

[19] J. Kuo and O. T. von Ramm, "Three-dimensional motion measurements using feature tracking," *IEEE Trans. Ultrason. Ferroelectr. Freq. Control*, vol. 55, no. 4, pp. 800–810, Apr. 2008.

[20] G. R. Bashford and O. T. von Ramm, "Ultrasound three-dimensional velocity measurements by feature tracking," *IEEE Trans. Ultrason. Ferroelectr. Freq. Control*, vol. 43, no. 3, pp. 376–384, May 1996.

[21] G. R. Bashford and D. J. Robinson, "Direct comparison of feature tracking and autocorrelation for velocity estimation," *IEEE Trans. Ultrason. Ferroelectr. Freq. Control*, vol. 54, no. 4, pp. 757–767, Apr. 2007.

[22] A. A. Morsy and O. T. von Ramm, "FLASH correlation: A new method for 3-D ultrasound tissue motion tracking and blood velocity estimation," *IEEE Trans. Ultrason. Ferroelectr. Freq. Control*, vol. 46, no. 3, pp. 728–736, May 1999.

Tiantian Xu received the B.S. degree in biomedical engineering from the Huazhong University of Science and Technology, Wuhan, PRC, in 2007. He is currently working as a Ph.D. student in the Department of Biological Systems Engineering at the University of Nebraska. His current research focuses on new methods of blood flow measurement, including feature tracking and speckle size estimation.

Gregory R. Bashford (M'96–SM'03) received the B.S. degree in electrical engineering from the University of Nebraska, Lincoln, NE, in 1991 and the Ph.D. degree in biomedical engineering from Duke University, Durham, NC, in 1995. He was previously an image analysis engineer at Acuson Corporation, Mountain View, CA; systems engineer at GE Medical Systems, Milwaukee, WI; and senior scientist at LI-COR Biosciences, Lincoln, NE. In 2003, he joined the faculty of the Biological Systems Engineering Department at the University of Nebraska. His research interests include methods and applications of biological and biomedical signal and image analyses.